J. Fluid Mech. (2011), *vol.* 678, *pp.* 248–270.
doi:10.1017/jfm.2011.110

Two-phase gravity currents in porous media

MADELEINE J. GOLDING†, JEROME A. NEUFELD, MARC A. HESSE AND HERBERT E. HUPPERT

Department of Applied Mathematics and Theoretical Physics, Institute of Theoretical Geophysics, University of Cambridge, Wilberforce Road, Cambridge CB3 0WA, UK

(Received 15 October 2010; revised 20 January 2011; accepted 2 March 2011; first published online 26 April 2011)

We develop a model describing the buoyancy-driven propagation of two-phase gravity currents, motivated by problems in groundwater hydrology and geological storage of carbon dioxide (CO_2). In these settings, fluid invades a porous medium saturated with an immiscible second fluid of different density and viscosity. The action of capillary forces in the porous medium results in spatial variations of the saturation of the two fluids. Here, we consider the propagation of fluid in a semi-infinite porous medium across a horizontal, impermeable boundary. In such systems, once the aspect ratio is large, fluid flow is mainly horizontal and the local saturation is determined by the vertical balance between capillary and gravitational forces. Gradients in the hydrostatic pressure along the current drive fluid flow in proportion to the saturation-dependent relative permeabilities, thus determining the shape and dynamics of two-phase currents. The resulting two-phase gravity current model is attractive because the formalism captures the essential macroscopic physics of multiphase flow in porous media. Residual trapping of CO_2 by capillary forces is one of the key mechanisms that can permanently immobilize CO_2 in the societally important example of geological CO_2 sequestration. The magnitude of residual trapping is set by the areal extent and saturation distribution within the current, both of which are predicted by the two-phase gravity current model. Hence the magnitude of residual trapping during the post-injection buoyant rise of CO_2 can be estimated quantitatively. We show that residual trapping increases in the presence of a capillary fringe, despite the decrease in average saturation.

Key words: gravity currents, multiphase flow, porous media

1. Introduction

The buoyancy-driven flow of immiscible fluids within a porous medium is a fundamental process that has applications to a host of engineering and environmental systems. In all cases, the interfacial tension acting between the fluids gives rise to a two-phase region over which the saturation, or pore volume fraction, of each fluid can vary. The model problem considered in § 4 is applicable to perched aquifers, which are formed when water in the subsurface accumulates on top of an impermeable barrier above the main water table in the partially saturated vadose zone (Fetter 2001). Another example is the migration, immobilization and reclamation of toxic substances such as chlorinated solvents and trichloroethylene, often referred to collectively as

† Email address for correspondence: mjg88@cam.ac.uk

dense non-aqueous phase liquids (DNAPLs). A related problem is the migration of light non-aqueous phase liquids (LNAPLs) in the capillary zone above the water table. In this case, three phases (air, water and LNAPL) flow in the pore space and similar concepts to those presented here apply (Parker & Lenhard 1989; Bear *et al.* 1996; Bear & Ryzhik 1998). Here we consider a two-phase gravity current resulting when a wetting phase, such as water, and a non-wetting phase, such as CO_2 or oil, are confined by an impermeable boundary in the porous medium and driven predominately horizontally by the density difference between the fluids.

One particularly timely and pressing example of two-phase flows in porous media is the geological storage of CO_2. Carbon capture and storage (CCS) is currently the only proposed technological means to reduce CO_2 emissions from fossil fuel power plants (Metz *et al.* 2005). The CO_2 is captured at source, compressed and injected into porous geological formations at least 1 km underground. Potential storage sites include saline aquifers, depleted oil reservoirs and unprofitable coal seams. Here we focus on saline aquifers, which provide the largest potential storage volume. In siliciclastic aquifers, which are mostly composed of silicate minerals, the aqueous brine is typically the wetting phase and the injected supercritical CO_2 is the non-wetting phase. The supercritical CO_2 is less dense than the ambient brine, so the buoyant CO_2 rises as a plume until it reaches a flow barrier, at which point it spreads laterally as a gravity current. The CO_2 continues to spread until either it is able to rise towards the surface, or it becomes permanently trapped by three main mechanisms listed here in order of increasing time scales (Metz *et al.* 2005): *residual trapping* where CO_2 is immobilized in pore spaces by capillary forces once injection has ceased; *solubility trapping* where CO_2 dissolves into brine to form a denser fluid that sinks and *mineral trapping* where CO_2 precipitates as minerals.

The long-term security of geological CO_2 storage is determined by the competition between leakage and trapping mechanisms (Nordbotten *et al.* 2005; Woods & Farcas 2009; Neufeld, Vella & Huppert 2009). In their study of the distribution of existing and abandoned wells in the oil-producing Alberta Basin, Gasda, Bachu & Celia (2004) highlight the large number of potential leakage pathways located in otherwise attractive CO_2 storage sites. This emphasizes the importance of trapping mechanisms that reduce the amount of CO_2 that is free to potentially escape, and the dependence of the security of long-term storage on trapping processes. Capillary forces can have significant effects on the migration and trapping of the CO_2 injected into geological formations saturated with brine.

Drainage occurs when the non-wetting fluid displaces the wetting fluid within the pore space and imbibition describes the opposite process. In both cases, a finite fraction of the displaced fluid generally remains in the pores and may become immobile. During drainage, the wetting phase remains within the pores as continuous thin films coating grain surfaces. During imbibition, the remaining fraction of the non-wetting phase is known as the residual saturation and is immobilized by capillary forces in the form of isolated ganglia. The residual trapping of the non-wetting fluid can be a problem in situations such as oil extraction or chemical spills because it can be difficult to remove much of the non-wetting phase efficiently. In contrast, capillary forces may have a positive influence on the long-term trapping of CO_2 during geological storage. During injection of the non-wetting CO_2, capillary forces both reduce the CO_2 saturation within the current and increase the vertical extent of the current. This increases the volume of reservoir and brine contacted by CO_2 and is therefore beneficial for dissolution and mineral trapping (Ennis-King & Paterson 2005; Riaz & Tchelepi 2006). When injection ceases, residual CO_2 is trapped as the

current proceeds through the formation. The saturation of CO_2 within the current during the injection stage greatly affects the amount that is subsequently trapped, and experimental work quantifies this dependence through initial–residual curves (Pentland *et al.* 2008). Previous gravity current models have assumed a constant, uniform CO_2 saturation and hence a constant amount of residual trapping (Hesse, Orr & Tchelepi 2008; Farcas & Woods 2009; MacMinn & Juanes 2009). Whilst these models capture the dependence of residual trapping on the areal extent of the current, the observed relationship between initial and residual saturations is not captured in estimates obtained in this way.

Many studies of gravity currents in porous media use a sharp-interface approximation, in which the regions within and without the current are fully saturated, and the two fluids are separated by a macroscopically sharp interface (Huppert & Woods 1995; Hesse *et al.* 2007; Gasda, Nordbotten & Celia 2009; Juanes, MacMinn & Szulczewski 2010). Such models, which predict the evolution of the current height h, were originally developed and tested for miscible flows in porous media and are applicable to two-phase gravity currents only when capillary forces are negligible compared to gravitational and viscous forces. Sharp-interface models have been developed for gravity currents in confined geometries ($h \sim H$, where H is the thickness of the reservoir), where the flow of both fluids is non-negligible, and hence the viscosity ratio plays a key role in their behaviour (Nordbotten & Celia 2006; Hesse *et al.* 2007; Neufeld & Huppert 2008; Juanes *et al.* 2010). For sharp-interface gravity currents in unconfined aquifers ($h \ll H$), there is negligible flow of the ambient fluid, and hence models of their propagation are independent of the ratio of viscosities between the fluids (Huppert & Woods 1995; Vella & Huppert 2006; Golding & Huppert 2010). However, when the two fluids are different phases, capillary forces may lead to a saturation transition zone that is not negligible, thus rendering the sharp-interface assumption invalid. In the particular case of CO_2–brine systems, the potentially large unstable viscosity contrast could further increase the size of the transition zone, or capillary fringe. Furthermore, sharp-interface models do not capture the strong reduction in relative permeability experienced by the non-wetting phase current, which could greatly affect predictions for its spreading velocity (Bickle *et al.* 2007). This provides an important motivation for the systematic development of a two-phase gravity current model and its analysis.

In this paper, we consider the buoyancy-driven propagation of immiscible fluids within a semi-infinite porous medium, taking explicit account of the effects of capillarity on the propagation and saturation within the current. In § 2 we introduce the standard formulation of two-phase flow in porous media (Pinder & Gray 2008). We use the large aspect ratio of the current to show that vertical velocities are negligible and that the saturation distribution is determined by vertical gravity–capillary equilibrium (Lake 1996). Hence, in § 3 we derive a two-phase gravity current model from the full governing equations. We find that the effect of capillary forces on the behaviour of the current is controlled by two nonlinear functions, which describe the dependence of the vertically integrated phase volume and flux on the thickness of the current. In § 4 we apply our model to steady-state gravity currents that form beneath discontinuous horizontal flow barriers during the buoyant rise of CO_2 through heterogeneous geological formations (Johnson, Nitao & Knauss 2004; Green & Ennis-King 2010; Hesse & Woods 2010) and estimate the magnitude of residual trapping. We conclude in § 5 with a discussion of the effect of two-phase phenomena on the behaviour of buoyant currents within the subsurface and provide an outlook for future research.

2. The standard model of two-phase flow in porous media

We consider the invasion of a non-wetting fluid into a porous medium that is initially saturated with a wetting fluid in a drainage process. In the following section, we summarize the standard two-phase model, which is based on the concept of macroscopic capillarity (Leverett 1941). The model considers the effects of interfacial tension and the reduction in fluid flow caused by the convoluted interface of the two fluids within the porous matrix on a scale much larger than the typical pore scale. Both fluid phases are considered to be immiscible and incompressible Newtonian liquids of constant, though unequal, density and viscosity. The action of capillary forces on the pore scale results in only a partial displacement of the wetting phase, and so the two phases co-exist within the same pore spaces. We denote quantities pertaining to the wetting and non-wetting phases by subscripts w and n respectively. The saturation, S_i, is a macroscopic quantity that describes the average volume fraction, ϕ_i, of phase i in a representative elementary volume (REV), normalized by porosity ϕ, i.e.

$$S_i = \phi_i/\phi, \quad i = w, n. \tag{2.1}$$

This definition implies the saturation constraint

$$S_w + S_n = 1. \tag{2.2}$$

The irreducible wetting phase saturation, denoted by S_{wi}, is the wetting phase saturation that always remains within the pores during drainage and is assumed to be constant. Two-phase flow models are therefore generally written in terms of an effective non-wetting phase saturation, s, and wetting phase saturation $1 - s$, defined by

$$s = \frac{S_n}{1 - S_{wi}} \quad \text{and} \quad 1 - s = \frac{S_w - S_{wi}}{1 - S_{wi}}. \tag{2.3}$$

The capillary pressure caused by the surface tension at the interface between two phases is expressed on the macroscopic scale by the difference in the pressure between phases,

$$p_n - p_w = p_c(s), \tag{2.4}$$

where the standard model assumes that the capillary pressure, p_c, is a function of saturation only.

In a drainage process, a minimum capillary pressure, called the capillary entry pressure, must be achieved for the non-wetting phase to enter a pore. The magnitude of the capillary entry pressure is inversely proportional to the size of the entrance to the pore. This entry pressure can create flow barriers for the non-wetting phase in regions where the porosity is reduced. As the capillary pressure increases, successively smaller pores are invaded. Typical $p_c(s)$ curves for a primary drainage process, where the non-wetting phase is invading the porous medium for the first time, are displayed in figure 1(a) for rock types with different pore-size distributions. If the porous medium has a narrow pore-size distribution (solid curve), once the capillary pressure is above the entry threshold for the largest pore, a small increase will be sufficient for the non-wetting phase to enter the majority of the remaining pores, and so the wetting phase saturation decreases rapidly. A wider distribution of pore sizes will result in a more gradual transition, as demonstrated in figure 1(a) (dash-dotted curve).

Two commonly used empirical models for capillary pressure curves are the Brooks–Corey and van Genuchten models (Brooks & Corey 1964; van Genuchten 1980). The derivation of the two-phase gravity current model presented here is independent of the specific parameterization of the capillary pressure curve. However, we choose the

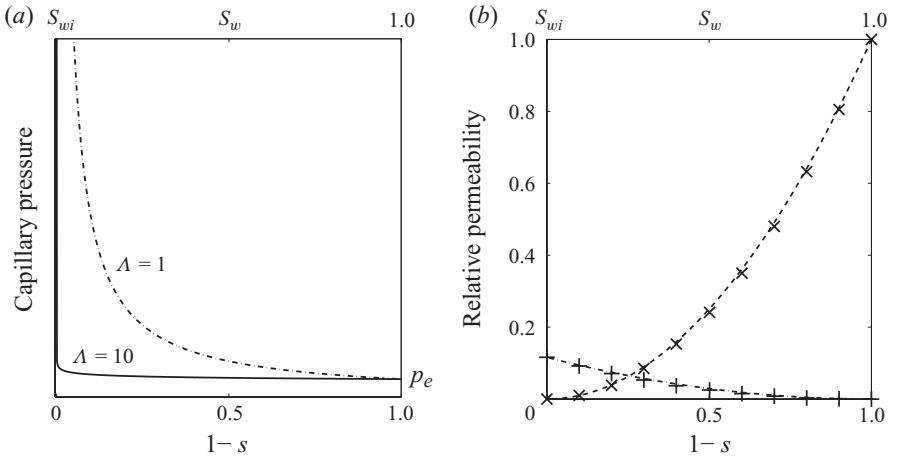

FIGURE 1. (*a*) Typical capillary pressure curves for drainage in porous media with narrow (solid curve) and wide (dash-dotted curve) pore-size distributions. (*b*) Non-wetting (+) and wetting (×) phase relative permeability data for Ellerslie Sandstone in the Alberta Basin, Canada, compared to typical model values with $\alpha = 2$ and $k_{rn0} = 0.116$ for the non-wetting (dash-dotted curve) and $\beta = 2$ for the wetting (dashed curve) phases. Data source: Bennion & Bachu (2005).

simpler Brooks–Corey curve to illustrate the model in order to minimize the number of parameters and because it is the more appropriate curve for consolidated rocks with a well-defined entry pressure. The Brooks–Corey capillary pressure function is given by

$$p_c = p_e(1-s)^{-1/\Lambda}, \tag{2.5}$$

where Λ is a fitting parameter related to the pore-size distribution. A small value of Λ corresponds to a wide distribution of pore sizes, whereas in the limit $\Lambda \to \infty$, all pores are of the same size. Examples of this curve are plotted in figure 1(*a*) for $\Lambda = 1$ and 10. The parameter p_e can be understood as the capillary pressure required for the non-wetting phase to enter the largest pores.

Local mass conservation in each phase requires

$$\phi \frac{\partial}{\partial t}(S_i) + \nabla \cdot \boldsymbol{u}_i = 0, \quad i = w, n, \tag{2.6}$$

where $\boldsymbol{u}_i$ is the volumetric flux of phase i. The extension of Darcy's law to two-phase flow (Leverett 1941) assumes that

$$\boldsymbol{u}_i = -k\lambda_i \left[\nabla p_i - \rho_i \boldsymbol{g}\right], \quad i = w, n, \tag{2.7}$$

where k is the intrinsic permeability of the porous medium, $\boldsymbol{g}$ is the gravitational acceleration, ρ_i is the density of phase i and p_i is the pressure averaged over a REV of phase i. The mobility of each phase,

$$\lambda_i(s) = k_{ri}(s)/\mu_i, \tag{2.8}$$

is inversely proportional to the dynamic viscosity, μ_i, and proportional to the relative permeability, k_{ri}, of each phase, which is assumed to be a unique nonlinear function of s only, during primary drainage. The presence of two phases alters both the pore space geometry and microscopic boundary conditions for each fluid, thereby changing the fluid flux in each phase which results from the application of a pressure gradient.

To account for this on the macro-scale, the relative permeability, k_{ri}, of each phase is a dimensionless scaling factor that multiplies the intrinsic permeability of the medium, k (Leverett 1939).

An approximate relationship for $k_{ri}(s)$ is commonly based on a power law (Corey 1954) of the effective saturation (2.3). Hence, we write the relative permeability of the non-wetting phase as

$$k_{rn} = k_{rn0}s^{\alpha}, \tag{2.9}$$

and of the wetting phase as

$$k_{rw} = (1-s)^{\beta}, \tag{2.10}$$

for some powers α and β, where $k_{rn0} < 1$ is the end point relative permeability of the non-wetting phase at its maximum saturation $s = 1$. When $s = 1$, the wetting phase is at the irreducible saturation, and is still hydraulically connected in the sense that Darcy flow could still occur via thin films. However, the effective permeability of the wetting phase is approximately zero since the fluid films are too thin for flow to be induced by the application of a typical pressure gradient. A review of various models used for the constitutive relations for consolidated rocks is given by Li & Horne (2006). Laboratory data for CO_2 in Ellerslie standstone, obtained by Bennion & Bachu (2005), are plotted in figure 1(*b*) along with the model values with $\alpha = \beta = 2$ and $k_{rn0} = 0.116$, which show excellent agreement. In this paper we consider flow in unconfined reservoirs for which fluid motion in the wetting phase can be neglected. Therefore, we require an expression only for the non-wetting phase relative permeability, and for this we set $\alpha = 2$ where necessary to enable analytical and numerical calculations. However, we emphasize that the model requires only $k_{rn} = k_{rn}(s)$ and is by no means restricted to this value of α.

Equations (2.2), (2.4) and (2.6)–(2.8), along with the constitutive relations (2.5), (2.9) and (2.10), form a complete description of two-phase flow. The capillary entry pressure, p_e, and pore-size distribution parameter, Λ, in the Brooks–Corey capillary pressure model, along with the relative permeability parameters α, β and k_{rn0}, are determined by fitting (2.5), (2.9) and (2.10) to experimental data. The irreducible wetting phase saturation, S_{wi}, embedded in the definition of effective saturation (2.3), must also be determined experimentally.

3. Development of a two-phase gravity current model

We now consider the buoyancy-driven flow of non-wetting fluid along a horizontal barrier and develop a vertically integrated model for a two-phase gravity current. As the current propagates, the non-wetting phase displaces the wetting phase which initially fills the pores in a primary drainage process. Fed by a constant flux per unit width q, the gravity current propagates beneath an impermeable upper boundary in an infinite reservoir initially fully saturated with a denser, wetting, fluid. This scenario is applicable to CO_2 spreading beneath an upper boundary of impermeable rock in a CO_2 storage reservoir as well as the migration of non-aqueous phase contaminants. The current height, $h(x,t)$, denotes the depth below which no non-wetting phase is present and where the non-wetting phase saturation drops to zero, $s = 0$ (see figure 2). The depth of the reservoir is much greater than the height of the current, and so the horizontal pressure gradient and the velocity in the wetting phase are negligible below the current. We additionally assume that the fluids are simply connected which implies that, to leading order, there are no horizontal pressure gradients driving flow of the wetting phase within the current.

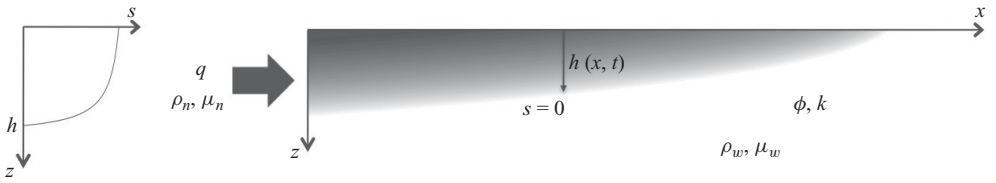

FIGURE 2. Sketch showing a gravity current with a non-uniform saturation profile propagating beneath an upper impermeable boundary into a porous medium saturated by fluid of a different phase, density and viscosity. The plot on the left shows a representative profile of saturation with depth.

3.1. *Vertical gravity–capillary equilibrium and saturation profile*

The dominant balance governing two-phase gravity currents can be found by applying scaling arguments in a manner analogous to previous studies of single-phase gravity currents (Huppert & Woods 1995, for example). For a current whose length L is much greater than its height H, i.e. $\epsilon = H/L \ll 1$, local mass conservation, as expressed by (2.6), implies that the vertical velocities are much less than the horizontal non-wetting phase velocity. Thus, the pressure within each phase is nearly hydrostatic and given by

$$\frac{\partial p_n}{\partial z} = \rho_n g \quad \text{and} \quad \frac{\partial p_w}{\partial z} = \rho_w g. \tag{3.1}$$

Pressures p_n and p_w are plotted in figure 3(a), where the difference at the current boundary $z = h$ is equal to the capillary entry pressure p_e. Consequently, (2.4) implies that

$$\frac{\partial p_c}{\partial z} = -\Delta\rho g, \tag{3.2}$$

where $\Delta\rho = \rho_w - \rho_n$, which mathematically captures the balance between gravitational and capillary forces within the current, known as vertical gravity–capillary equilibrium. We integrate (3.2) between z and h to obtain the expression for capillary pressure as a function of height

$$p_c[h(x,t), z] = p_e - \Delta\rho g(z - h), \tag{3.3}$$

where we note that the capillary pressure at the edge of the current $p_c(z = h) = p_e$.

The assumption of gravity–capillary equilibrium is commonly invoked in studies of multiphase flow (Yortsos 1995; Lake 1996, for example). In this study, it follows from the large aspect ratio of the gravity current and the subsequent assumption that pressure within each phase is hydrostatic. We expand on this assumption in the Appendix and show that the time scale over which gravity–capillary equilibrium is recovered during the motion of the current is much smaller than the time scale for the motion itself. In this way, we show that the assumption remains valid as the current propagates. We note that the assumption breaks down in areas where saturation is very low (Lake 1996). In this region, which is located along the current boundary, the relative permeability of the non-wetting phase is very small, leading to potentially long time scales for recovering gravity–capillary equilibrium as the current propagates. However, this region is thin, and we anticipate that the behaviour within it has little influence on the overall motion of the current predicted by our vertically integrated model.

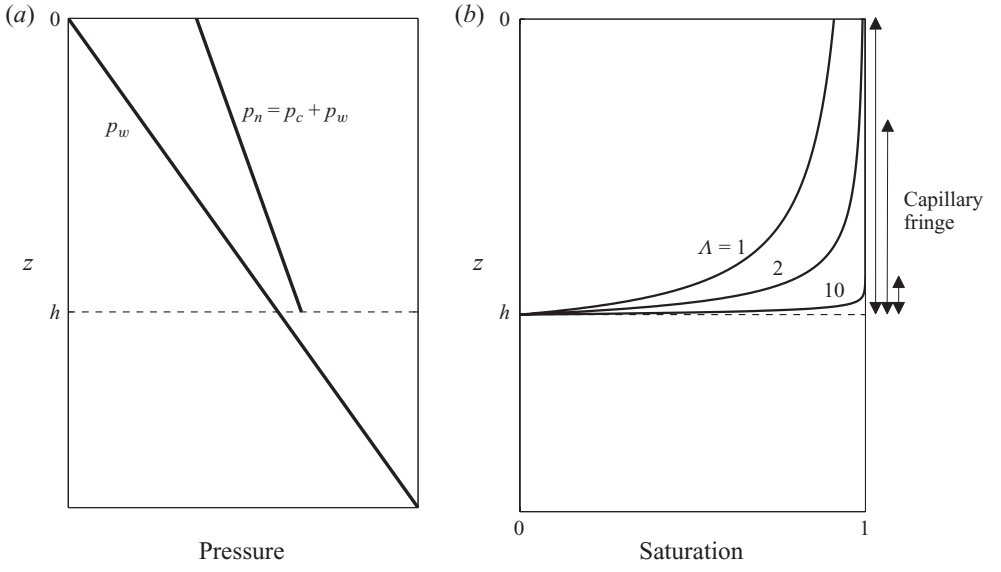

FIGURE 3. (*a*) Graph illustrating the hydrostatic pressure within each fluid. The difference between the non-wetting and wetting phase pressures at $z = h$ is equal to the capillary entry pressure p_e. (*b*) Saturation profiles within the current are plotted for $\Lambda = 1,\ 2$ and 10. The size of the capillary fringe or transition zone, where the non-wetting phase saturation varies considerably, is indicated by arrows for each case.

Parker & Lenhard (1989) combine an expression for capillary pressure resulting from the gravity–capillary equilibrium assumption in three-phase flow, analogous to (3.3), with the Brooks–Corey model, to find the implied wetting phase saturation as a function of vertical position. Here we treat the simpler two-phase case similarly by equating (2.5) and (3.3), to obtain an expression for the non-wetting phase saturation, s, within the gravity current as a function of h and z given by

$$s[h(x,t),z] = 1 - \left(1 + \frac{h-z}{h_e}\right)^{-\Lambda}, \tag{3.4}$$

where the length scale h_e is defined by

$$h_e \equiv p_e/\Delta\rho g. \tag{3.5}$$

The saturation profile given by (3.4), which is a function of h and z, is plotted in figure 3(*b*). Physically, the capillary entry height, h_e, represents the height of a column of non-wetting fluid such that the hydrostatic pressure equals the entry pressure of the largest pore throat found in the porous medium. It is therefore a measure of the relative strength of capillary forces to gravitational forces. The region in which the non-wetting phase saturation varies considerably is referred to as the transition zone, or capillary fringe. The width of the capillary fringe increases with the magnitude of capillary forces, i.e. with the inverse of the pore-size distribution parameter $1/\Lambda$ (as shown in figure 3*b*) and with the capillary entry height h_e. Bear *et al.* (1996) define a similar height to h_e, which is often used as a characteristic length scale for the capillary fringe in a three-phase system.

3.2. *Vertically integrated equation for the current height profile*

Vertical integration of (2.6) for the non-wetting phase between $z=0$ and $z=h$ yields

$$\varphi\left(\frac{\partial}{\partial t}\int_0^h s\,\mathrm{d}z - s(h)\frac{\partial h}{\partial t}\right) + \frac{\partial}{\partial x}\int_0^h u_n\,\mathrm{d}z - [u_n]_{z=h}\frac{\partial h}{\partial x} + [w_n]_0^h = 0, \tag{3.6}$$

where $\varphi=\phi(1-S_{wi})$. This reduces to

$$\varphi\frac{\partial}{\partial t}\int_0^h s\,\mathrm{d}z + \frac{\partial}{\partial x}\int_0^h u_n\,\mathrm{d}z = 0, \tag{3.7}$$

since $s(h)=0$ and $\lambda_n[s(h)]=0$ at the edge of the current, and therefore, by (2.7), the non-wetting phase velocities $u_n=w_n=0$ at $z=h$. We impose the condition $w_n=0$ on the upper impermeable boundary at $z=0$. This equation was derived by Bear & Ryzhik (1998) to describe a DNAPL lens moving over an impermeable boundary.

The first integral in (3.7) is calculated directly using (3.4). We substitute (2.7) into the second integral and therefore find that (3.7) becomes

$$\varphi\left[1-\left(1+\frac{h}{h_e}\right)^{-\Lambda}\right]\frac{\partial h}{\partial t} - k\Delta\rho g\frac{\partial}{\partial x}\left[\frac{\partial h}{\partial x}\int_0^h \lambda_n\,\mathrm{d}z\right] = 0. \tag{3.8}$$

This can be further simplified by noting that the non-wetting phase saturation at the upper boundary $z=0$ can be expressed by the saturation function

$$s_0(h/h_e) \equiv s(h/h_e, z=0) = 1-\left(1+\frac{h}{h_e}\right)^{-\Lambda}. \tag{3.9}$$

Hence, we obtain the principal new equation that governs the flow of a two-phase buoyancy-driven current,

$$\varphi s_0(h/h_e)\frac{\partial h}{\partial t} - \frac{\Delta\rho g\tilde{k}}{\mu_n}\frac{\partial}{\partial x}\left[h\frac{\partial h}{\partial x}\mathscr{F}(h/h_e)\right] = 0, \tag{3.10}$$

where $\tilde{k}=kk_{rn0}$. Here, the effect of the vertical saturation distribution on flow due to variation in relative permeability is encapsulated in the flux function

$$\mathscr{F}(h/h_e) \equiv \frac{\mu_n}{k_{rn0}h}\int_0^h \lambda_n[s(z)]\,\mathrm{d}z \tag{3.11}$$

$$= \frac{h_e}{\Lambda h}\int_0^{s_0(h/h_e)} S^{\alpha}(1-S)^{-(\Lambda+1)/\Lambda}\,\mathrm{d}S. \tag{3.12}$$

To obtain (3.12), we change variables from z to s (defined by (3.4)) by noting that $\partial s/\partial z = -(\Lambda/h_e)(1-s)^{(\Lambda+1)/\Lambda}$. It may be interesting to note that the integral in (3.12) is, in fact, the incomplete beta function, defined as $\mathscr{B}(x:a,b)\equiv\int_0^x u^{a-1}(1-u)^{b-1}\,\mathrm{d}u$, with $x=s_0(h/h_e)$, $a=1+\alpha$ and $b=-1/\Lambda$. We are able to integrate (3.12) directly

when $\alpha = 2$ to find an analytical expression for $\mathscr{F}$ given by

$$\mathscr{F}(h/h_e) = \frac{h_e}{h}\begin{cases}\left[\dfrac{3s_0^2 - 2s_0}{(1-s_0)^2} - 2\log(1-s_0)\right] & (\Lambda = 0.5)\\ \left[\dfrac{s_0(2-s_0)}{1-s_0} + 2\log(1-s_0)\right] & (\Lambda = 1)\\ \left[\dfrac{(1-s_0)^{-1/\Lambda}}{1-2\Lambda}\left[s_0^2 + \dfrac{2\Lambda(s_0-\Lambda)}{\Lambda-1}\right] + \dfrac{2\Lambda^2}{(\Lambda-1)(1-2\Lambda)}\right] & (\Lambda \neq 0.5, 1),\end{cases} \tag{3.13}$$

where $s_0 = s_0(h/h_e)$, and we will use this in § 4.1.

The explicit framework encapsulated by (3.9), (3.10) and (3.12) represents a significant advance in our understanding of the effects that two-phase phenomena have on the propagation of gravity currents in porous media, accounting for the non-uniform saturation distribution of the fluid in the current. Equation (3.10) is the two-phase analogue of the sharp-interface models considered by a number of authors (Huppert & Woods 1995). The two-phase behaviour is captured by two functions of h/h_e, defined in (3.9) and (3.12). The flux function, $\mathscr{F}$, and the saturation function, s_0, are investigated further in § 3.3. We show that in the appropriate limits, $h/h_e \to \infty$ and $\Lambda \to \infty$, the two-phase functions $s_0(h/h_e) \to 1$ and $\mathscr{F}(h/h_e) \to 1$, and thus the single-phase governing equation is recovered. It is worth emphasizing the generality of (3.11), for which any function of saturation can be supplied for the non-wetting phase mobility, λ_n. We use a power relation for the non-wetting phase relative permeability in this study to illustrate the two-phase behaviour (Li & Horne 2006).

To complete the mathematical description of the problem, we specify two boundary conditions. The flux at the origin can be written as

$$\frac{\Delta\rho g\tilde{k}}{\mu_n} h \frac{\partial h}{\partial x}\mathscr{F}(h/h_e) = -q. \tag{3.14}$$

The second boundary condition recognizes that the height of the current at the nose, located at $x = x_N(t)$, is

$$h(x_N) = 0. \tag{3.15}$$

3.3. *The flux function, $\mathscr{F}(h/h_e)$, and saturation function, $s_0(h/h_e)$*

The flux function $\mathscr{F}(h/h_e)$, defined by (3.12), accounts for the depth-integrated relative permeability of the non-wetting phase and depends on the pore-size distribution parameter Λ, the capillary entry height he and the power α in the constitutive relationship (2.9). We focus on the effects of varying Λ and h_e in this paper in order to constrain the parameter space, and because the value $\alpha = 2$ is reasonable for many CO_2/brine systems, as demonstrated in figure 1(*b*) (Bennion & Bachu 2005).

Figure 4(*a*) shows a graph of $\mathscr{F}(h/h_e)$ for $\Lambda = 0.5$, 1, 2 and 10. For finite values of Λ, $\mathscr{F}$ is a monotonically increasing function of h/h_e, which tends to 1 as $h/h_e \to \infty$. This is due to the fact that when the current is much thicker than the capillary fringe, the non-wetting fluid nearly saturates the pores in most of the current, and so capillary effects become less important to its overall motion. The limit also corresponds to the case of negligible capillary entry pressure, i.e. $p_e \ll 1$. When h is comparable to or smaller than the capillary fringe, non-wetting phase saturations are lower, which results in reduced local relative permeabilities and hence lower values of $\mathscr{F}$.

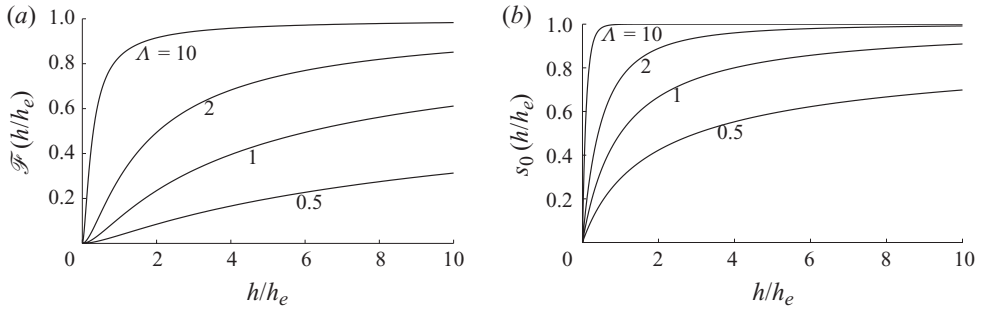

FIGURE 4. The flux function $\mathscr{F}(h/h_e)$, plotted in (a), and the saturation function $s_0(h/h_e)$, plotted in (b), are shown for $\Lambda = 0.5$, 1, 2 and 10.

The saturation function, $s_0(h/h_e)$, plotted in figure 4(b) for $\Lambda = 0.5$, 1, 2 and 10, indicates the thickness of the current with respect to the capillary fringe, which is defined as the depth over which the non-wetting fluid saturation in the current increases from $s = 0$ to some cut-off value $s = s_c \sim 1$. The width of the capillary fringe is the value of h for which $s_0(h/h_e) = s_c$. We can see clearly from figure 4(b) that the capillary fringe width increases with $1/\Lambda$ and h_e.

Thus, for all finite values of Λ, the current approaches the single-phase result, where $\mathscr{F} \equiv 1$ and $s_0 \equiv 1$, when $h/h_e \gg 1$. The rate of convergence to the single-phase limit increases with Λ because the capillary fringe is thinner. In the limit $\Lambda \to \infty$, which describes a medium of uniform pore size with a single capillary entry pressure, there are no capillary effects on the gravity current and $s_0 \equiv 1$ and $\mathscr{F} \equiv 1$ for all values of h/h_e.

Conversely, in the limit $\Lambda h/h_e \ll 1$, the saturation function is approximately linear in h, given by

$$s_0(h/h_e) \approx \Lambda h/h_e, \tag{3.16}$$

and $\mathscr{F}$ can be approximated as

$$\mathscr{F}(h/h_e) \approx \frac{1}{\alpha + 1}\left(\frac{\Lambda h}{h_e}\right)^{\alpha}. \tag{3.17}$$

4. An application to geological CO_2 storage

Many geological systems identified as potential sites for CO_2 storage are heterogeneous, containing nearly horizontal, discontinuous barriers to flow. Such barriers may include shale layers, which have a greatly reduced permeability, are regions of high capillary entry pressure, and are therefore effectively impermeable to the non-wetting phase. Johnson *et al.* (2004) identified these ubiquitous shale layers as having a crucial effect on migration and trapping of CO_2 in storage reservoirs such as Sleipner. More recently, Saadatpoor, Bryant & Sepehrnoori (2010) showed that capillary barriers can have a dominant effect on CO_2 migration and trapping. The enhanced lateral dispersion due to discontinuous shales is important for residual trapping because it causes the CO_2 to contact a larger volume of the reservoir (Johnson *et al.* 2004; Hesse & Woods 2010). The 'inject low and let rise' strategy for geological CO_2 storage (Kumar *et al.* 2005; Bryant, Lakshminarasimhan & Pope 2008) tries to maximize the dispersion and trapping of CO_2 due to flow barriers, by injecting it through a horizontal well at the base of the storage formation (figure 5).

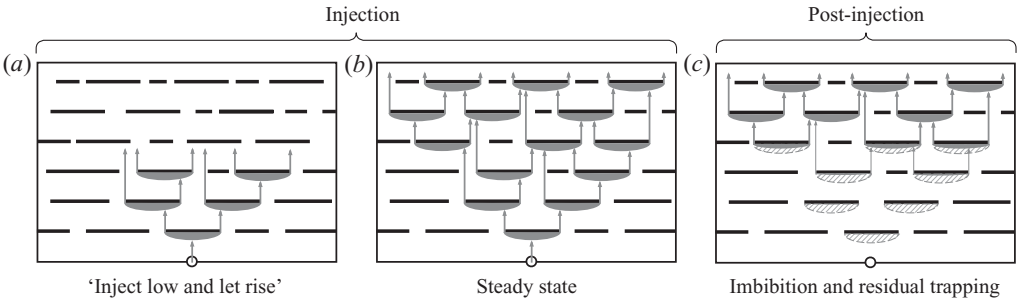

FIGURE 5. Sketch showing the three stages of injecting CO_2 into a storage reservoir. Figure (*a*) depicts the early stages of injection where CO_2 starts to rise through a geological formation containing shale layers. In figure (*b*) the gravity currents that form beneath each shale layer have reached a steady state. Figure (*c*) sketches the post-injection stage where CO_2 is residually trapped in regions previously occupied by the non-wetting phase gravity currents.

We envisage the following idealized scenario, shown schematically in figure 5. Injection at the base of a heterogeneous formation begins with the rise of buoyant CO_2 through the permeable pore space (figure 5*a*). As the CO_2 rises, it encounters horizontal barriers to flow and spreads laterally (figure 5*b*), which has important implications for the lateral dispersal and numerical upscaling of the reservoir, as discussed in Hesse & Woods (2010) and Green & Ennis-King (2010). The CO_2 perched beneath each barrier forms a steady-state gravity current. At the end of the injection period (figure 5*c*), fluid continues to rise throughout the system, leaving residual CO_2 trapped in its wake. In this scenario, residual trapping occurs most notably in the regions beneath flow barriers, previously occupied by steady-state CO_2 plumes that can be modelled as gravity currents.

The volume of CO_2 that is residually trapped during this final stage is of primary importance for the long-term safe storage of CO_2 within the subsurface because it leads to rapid immobilization of CO_2 after the end of injection. The quantity trapped depends on two key factors, both of which are influenced by two-phase phenomena: the volume of rock invaded by CO_2 in the reservoir and the saturation within the contacted region. Experimental data indicate that the residual saturation, $S_{n,res}$, depends on the initial saturation of the non-wetting phase, $S_{n,init}$, at the time of flow reversal (Pentland *et al.* 2008). Therefore, the amount of CO_2 immobilized by capillary forces and the rate of trapping depends on the saturation distribution of the non-wetting CO_2 at the end of the injection phase.

At leading order, the buoyant rise of CO_2 through a series of flow barriers can be understood by studying the steady current beneath a single layer (Hesse & Woods 2010). Therefore, we focus on the buoyancy-driven flow of non-wetting fluid beneath a single barrier (figure 6). For continuous injection, we anticipate that the gravity currents will reach a steady state after sufficient time, in which the flux into the current equals the flux rising at the ends. In § 4.1 we investigate how capillary forces affect the vertical extent and saturation distribution within a gravity current beneath a single impermeable barrier. The height and saturation profiles obtained in § 4.1 are then used as inputs to a trapping model, which captures the relationship between initial and residual saturations. In this way, we are able to gain valuable insight into how capillary forces affect the magnitude of residual trapping in the 'inject low and let rise' strategy for CO_2 storage.

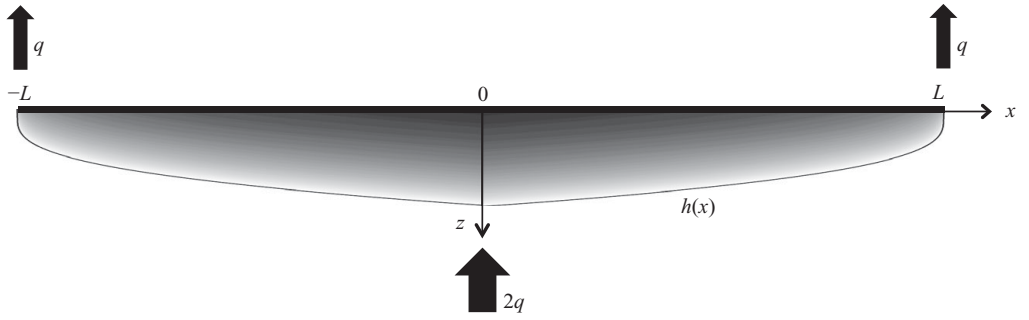

FIGURE 6. Sketch of a steady-state two-phase gravity current beneath a barrier of finite extent. Injection of a flux $2q$ at $x=0$ is balanced exactly by vertical flow at $x=\pm L$, resulting in a steady-state current whose saturation we model with depth.

4.1. *Steady-state two-phase current beneath a finite boundary*

We consider a steady-state gravity current, under a barrier of finite length, $2L$, where L is much greater than the current height. Non-wetting fluid is injected with constant flux $2q$ at the centre of the barrier and spreads to the edges at $x=\pm L$, where it rises vertically from the system and so the edges effectively act as sinks. Due to the symmetry of the problem, we consider only half of the current sketched in figure 6 and solve for a current fed by a flux of magnitude q at $x=0$. We see from (3.10) that the profile of the steady state is given by

$$\frac{\mathrm{d}}{\mathrm{d}x}\left[h\frac{\mathrm{d}h}{\mathrm{d}x}\mathscr{F}\left(h/h_e\right)\right]=0, \tag{4.1}$$

with boundary conditions

$$\frac{\Delta\rho g\tilde{k}}{\mu_n}h\frac{\mathrm{d}h}{\mathrm{d}x}\mathscr{F}(h/h_e)=-q \quad (x=0), \tag{4.2a}$$

$$h=0 \quad (x=L). \tag{4.2b}$$

Unlike the case for unbounded spreading, there exists a natural horizontal length scale to our steady-state problem, L, and we define the corresponding vertical height scale

$$H=\left(\frac{q\mu_n L}{\Delta\rho g\tilde{k}}\right)^{1/2} \tag{4.3}$$

introduced by Huppert & Woods (1995). We define dimensionless variables

$$x'=x/L \quad \text{and} \quad h'=h/H, \tag{4.4}$$

but drop the primes for ease of notation in the subsequent analysis.

The existence of a third length scale, the capillary rise height h_e, is expressed in terms of a Bond number

$$B\equiv\frac{\Delta\rho g H}{p_e}=H/h_e, \tag{4.5}$$

which is the ratio of the hydrostatic pressure for a scale height H and the capillary entry pressure. It therefore indicates the relative importance of capillary forces compared to gravitational and viscous forces. The single-phase case is recovered in the limit $B\to\infty$ in which either the capillary entry pressure $p_e\to 0$ or the height of the current is sufficiently large that the capillary fringe is small in comparison.

Hence, after integration and application of the boundary condition at $x = 0$, the dimensionless governing equation is

$$h\frac{\mathrm{d}h}{\mathrm{d}x}\mathscr{F}(hB) = -1. \tag{4.6}$$

The remaining boundary condition is

$$h(x = 1) = 0, \tag{4.7}$$

and the flux function and saturation function are given by

$$\mathscr{F}(hB) = \frac{1}{B\Lambda h}\int_0^{s_0(hB)} S^{\alpha}(1-S)^{-(\Lambda+1)/\Lambda}\,\mathrm{d}S \tag{4.8}$$

and

$$s_0(hB) = 1 - (1+hB)^{-\Lambda} \tag{4.9}$$

respectively.

When $\alpha = 2$, we can use the analytical expressions for the function $\mathscr{F}(h)$, (3.13), to greatly simplify the governing equation for the current height. We make the expressions dimensionless using (4.4), substitute into the steady-state governing equation (4.6), integrate and rearrange, and hence obtain implicit algebraic expressions for h, displayed here for the values $\Lambda = 0.5$ and 1 used in figures 7(*c–f*),

$$2(1-x) = \begin{cases} h^2 + 6\dfrac{h}{B} + \dfrac{16}{3B^2}[1-(1+hB)^{3/2}] + \dfrac{2}{B^2}(1+hB)\log(1+hB) & (\Lambda = 0.5), \\ h^2 + 6\dfrac{h}{B} - \dfrac{2}{B^2}(3+2hB)\log(1+hB) & (\Lambda = 1). \end{cases} \tag{4.10}$$

In a similar manner, equations for other values of Λ can be derived, but due to their intricate nature, they are not displayed here. Hence, the steady-state height profile of a two-phase gravity current is the solution to a nonlinear algebraic equation.

We note that the solution for the height profile in this steady-state problem in the sharp-interface limit is

$$h = \sqrt{2(1-x)}, \tag{4.11}$$

which has been shown to fit experimental data in a Hele-Shaw cell very well (Hesse & Woods 2010). It is worth noting that when $B \to \infty$, the steady-state single-phase solution is recovered.

4.1.1. *The effect of pore geometry and capillary forces*

By studying this steady-state problem, much insight can be gained into the general influence of capillarity and pore-size distribution on two-phase gravity currents, as captured in our model by parameters B and Λ respectively. The pore-size distribution parameter Λ determines how quickly the saturation increases with distance from the current boundary. A series of plots in figure 7 shows non-wetting phase saturation profiles and distributions for $\Lambda = 0.5$, 1 and 10, where the Bond number $B = 1$ is held constant. When $\Lambda = 10$, the current approaches the sharp interface limit. In this case, figures 7(*a*) and 7(*b*) show that there is a small transition zone at the edge of the current. As Λ decreases and capillary effects become more important (figures 7*c–f*), the transition zone becomes larger. As this happens, the average saturation decreases, and consequently the current thickens in order to maintain the constant flux of injected fluid.

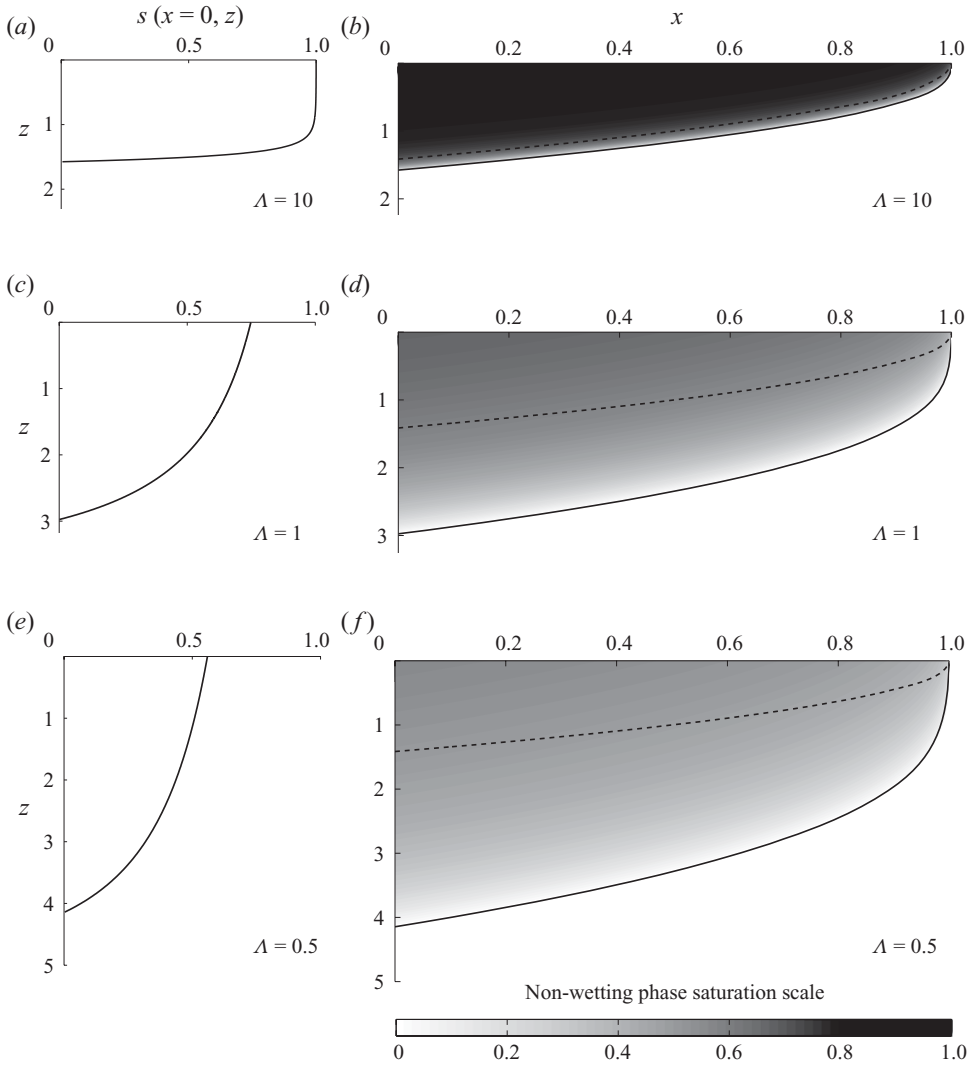

FIGURE 7. Saturation profiles and distributions for $B = 1$, with $\Lambda = 10$ (a,b), $\Lambda = 1$ (c,d) and $\Lambda = 0.5$ (e,f). Figures (a), (c) and (e) show the saturation at $x = 0$, and figures (b), (d) and (f) illustrate the shape and saturation within each current. In each case the solid line indicates $h(x)$, where $s(h) = 0$, and the dashed line indicates the sharp-interface limit.

The height of the current at the origin, $h_0 \equiv h(x = 0)$, as a function of Λ and B, is plotted in figures 8(a) and 8(b) respectively. We use the current height at the origin to give an indication of the areal extent of the current, which strongly influences the extent of residual trapping that can occur, as discussed in § 4.2. Both graphs demonstrate how increasing capillary effects, either by decreasing Λ or B, thicken the current. The effect of varying B on the average saturation within a current where $\Lambda = 1$ is summarized in figure 8(c).

It is not clear, *a priori*, how the opposing effects of a lower average saturation and a larger areal extent will affect the total volume of non-wetting fluid contained within the current. The graph in figure 8(d) shows the total volume of the non-wetting phase

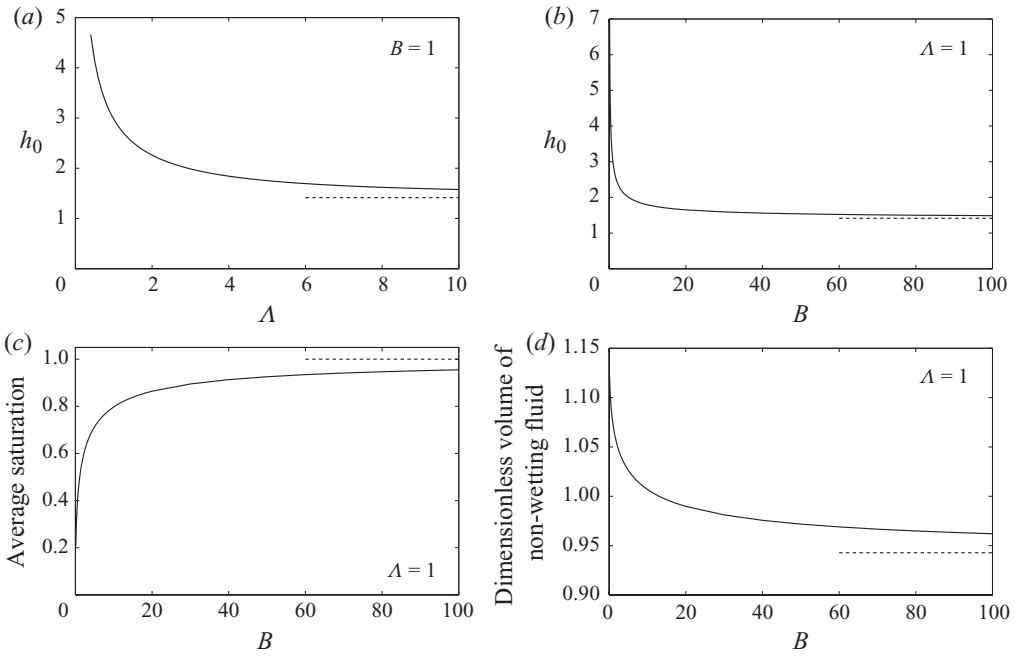

FIGURE 8. Figures (*a*) and (*b*) plot the current height at the origin, h_0, against Λ, with $B = 1$ and against B, with $\Lambda = 1$, respectively. Figures (*c*) and (*d*) plot respectively the average saturation and the total volume of non-wetting fluid contained within the steady-state current as functions of B, with $\Lambda = 1$. The dashed lines indicate the values in the sharp-interface limit.

as a function of B, for $\Lambda = 1$. We see that the volume always increases with increasing capillary forces.

We investigate in § 4.2 how both the volume of fluid contained in the currents and the saturation distribution affect estimates for residual trapping within the system.

4.2. *Residual trapping*

Residual trapping occurs when ganglia of the non-wetting phase become disconnected from the main bulk of the fluid and therefore immobilized during imbibition. It is caused by surface tension acting within the pore geometry, making it impossible for the wetting fluid to displace all of the non-wetting fluid. For detailed explanations of the mechanisms on the pore scale which cause residual trapping, the reader is directed towards Lenormand, Zarcone & Sarr (1983) and Pinder & Gray (2008).

At the macro-scale, the key experimental observation is the dependence of the non-wetting phase residual saturation on the initial saturation at the time of flow reversal (Land 1968). An initial–residual graph summarizing these data for a number of two-phase-rock systems studied in the literature can be found in figure 2 in Pentland *et al.* (2008). All the data sets have a common feature that a higher fraction of fluid is trapped in regions where the initial saturation is lower. Several models have been developed to represent these empirical measurements and a useful summary of these results is contained in figure 6 of Pentland *et al.* (2008).

The magnitude of residual trapping in the gravity currents considered in § 4.1 is primarily dependent on the areal extent of the current and the maximum saturation reached during the drainage stage, i.e. the steady-state height and saturation profile. This allows us to avoid modelling the details of the imbibition process when inferring

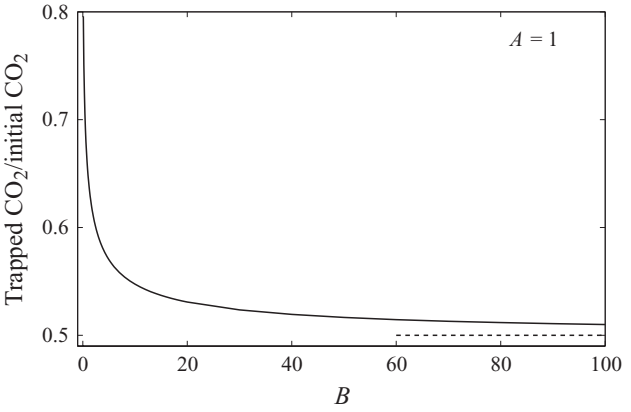

FIGURE 9. Fraction of fluid trapped residually, for $\Lambda = 1$, as a function of B estimated using Land's model with $C = 1$. The dashed line represents the estimate obtained by applying Land's model to a sharp-interface gravity current. Note that this limit is approached more quickly with respect to increasing B for higher values of Λ.

the volume of the residually trapped non-wetting phase and instead apply a trapping model directly to the steady-state saturations.

As an example, we use Land's model (Land 1968) to estimate the fraction of fluid that is trapped residually in the steady-state currents considered in § 4.1. Land's model relates initial and residual saturations by

$$S_{n,res} = \frac{S_{n,init}}{1 + C S_{n,init}}, \tag{4.12}$$

where C is known as Land's coefficient, and for application to a CO_2–brine–rock system, has a value of order 1 (Juanes *et al.* 2006). We apply this relation across the initial saturation profile calculated from the steady-state problem, integrate over the height and length of the current and thus calculate how much fluid would be trapped if the constant flux were turned off. Figure 9 presents estimates for the fraction of initial fluid in the steady-state current that would be residually trapped as a function of B, with $\Lambda = 1$. We compare this to estimates obtained using a sharp interface model, with $S_{n,init} = 1$ everywhere and find that including capillary effects can increase estimates for the fraction of CO_2 residually trapped by more than 50 %. We see this increase in the proportion of trapped fluid because the average saturation in the currents is lower. Furthermore, the actual volume of fluid contained in a current is larger with increased capillary forces, due to its greater areal extent (figure 8*d*), which means that a greater absolute volume of fluid is trapped.

5. Conclusions and discussion

One of the major difficulties of modelling the flow of CO_2 during geological storage is the range of scales over which processes occur. Full numerical simulations of flow (Kumar *et al.* 2005; Mo *et al.* 2005; Ide, Jessen & Orr 2007) are able to incorporate two-phase phenomena, but the computational intensity requires a compromise on spatial resolution. On the other hand, sharp-interface models lose small-scale details such as the saturation distribution but are able to model flow over much larger distances (Nordbotten & Celia 2006; Hesse, Orr Jr & Tchelepi 2008; Juanes *et al.*

2010). Many theoretical models of gravity currents in porous media to date have assumed a sharp interface separating the fluid in the current from the ambient (Huppert & Woods 1995; Hesse *et al.* 2007). This is appropriate in situations where capillary forces are negligible compared to viscous and gravitational forces. However, when the intruding and ambient fluids are different phases, capillary forces acting between them can have a significant influence on their motion. In this study, we considered the propagation of a gravity current of a non-wetting fluid, along an impermeable horizontal boundary, into a porous medium initially saturated by a wetting fluid. We assume that sufficient time has elapsed for the current to become long and thin. We model the resulting non-uniform saturation distribution and derived a vertically integrated, time-dependent equation that governs the height of the gravity current. The two-phase governing equation is analogous to its single-phase counterpart (Huppert & Woods 1995), with the two-phase effects incorporated by two new functions describing the saturation at the impermeable boundary and the vertically integrated flux through the current as a function of its height. We show that our two-phase model recovers the sharp-interface case in appropriate parameter limits. The two-phase framework is attractive because it captures the effects introduced by surface tension between the two fluids, whilst maintaining the form of the sharp-interface model.

The two key features to consider when modelling two-phase flow on the macro-scale are capillary pressure and relative permeability. The model developed in this paper captures the general functional dependence of both features on saturation. We illustrate this dependence by using the Brooks–Corey model for capillary pressure and power law relations for relative permeability. The central assumption is that of gravity–capillary equilibrium, where gravitational and capillary forces balance in the vertical direction, which we show to be valid for long, thin gravity currents. Using this assumption of gravity–capillary equilibrium, along with the capillary pressure as a function of saturation, we obtained an explicit expression for the saturation profile within the current. This profile depends primarily on the pore-size distribution, characterized by Λ, and the ratio of capillary to gravitational forces, characterized by h_e. We found that as both $1/\Lambda \to 0$ and $h_e \to 0$, capillary forces become negligible and the capillary fringe reduces to the sharp-interface limit. The effect of the saturation profile on the flow of a two-phase gravity current was encapsulated in the flux function $\mathscr{F}(h/h_e)$, which itself is a function of Λ and h_e. The value of the height scale h_e in geological settings varies widely depending on the rock and fluid types. For example, Bennion (2006) measured capillary entry pressures $p_e = 3.5$ kPa in a sandstone formation and $p_e = 493.6$ kPa in a carbonate formation in the Alberta Basin, Canada, which could potentially be suitable as sequestration sites. Using these values, along with $g = 9.8$ m s^{-2} and representative densities $\rho_w = 1020$ kg m^{-3} and $\rho_n = 550$ k gm^{-3} (Bickle *et al.* 2007), we calculate representative capillary entry heights of $h_e = 0.76$ m and 107 m respectively.

We used our model of a two-phase gravity current to assess the magnitude of residual trapping as a buoyant plume of CO_2 rises through a heterogeneous formation. By considering CO_2 ponded beneath a single, finite barrier, we were able to investigate how the main parameters influence the areal extent and non-uniform saturation profile of a two-phase gravity current. We demonstrated how capillary forces simultaneously thicken the current, i.e. increase its vertical extent, and reduce the average saturation within it. These two effects have opposing influences on the volume of fluid that accumulates in steady-state currents. We have shown that the net result in all cases studied is an increase with capillary forces in the volume of

non-wetting fluid contained within a current, indicating that the increased vertical extent dominates.

Residual trapping happens once injection of CO_2 ceases and is one of the key mechanisms enabling the success of long-term storage of CO_2 as part of the immense challenge of climate change mitigation. Some steps have been made towards incorporating the effects of residual trapping in sharp interface models, by assuming that the volume of fluid in the current decreases at a constant rate, controlled by a trapping parameter (Kochina, Mikhailov & Filinov 1983; Hesse *et al.* 2008; Juanes *et al.* 2010). With the two-phase model developed in this paper, we are able to investigate the extent of residual trapping more accurately because we know the height and saturation profiles at the end of the injection period. Whilst we use Land's trapping model to obtain estimates, it is important to note that any model relating initial–residual saturations could be used once the saturation profile is known. The essential feature that at lower saturations, the fraction of fluid trapped is higher is the reason why, as capillary effects are increased and the two-phase currents have lower average saturations, the fraction of fluid residually trapped is greater. Moreover, the amount of fluid contained in the steady-state current at the start of imbibition is larger when capillary forces are higher, so the overall volume of fluid trapped is also higher, not just the fraction. This result is important given that residual trapping post-injection is proportional to the volume of fluid per unit length in the steady current (Hesse *et al.* 2008). Furthermore, the increased height means a greater volume of rock is invaded by CO_2 as capillary effects are increased, and it is therefore able to contact a larger volume of brine, which could increase further trapping by dissolution (Johnson *et al.* 2004).

Whilst we have considered steady-state gravity currents in this paper, the model developed is fully time-dependent and therefore provides a theoretical framework in which to investigate how capillary forces affect the motion of transient two-phase gravity currents. For example, it is not clear how the reduced relative permeability at the nose of the current, caused by the lower saturation when the height decreases to zero, affects the steepness of the nose and the thickness and velocity of the entire current. Other future work will extend the methods outlined here to two-phase gravity currents propagating in a confined aquifer, where the viscosity ratio of the fluids plays an important role. Our framework also holds the promise of being able to model drainage and imbibition in a self-consistent manner, using differing capillary pressure and relative permeability relationships, thus improving the assessment of residual trapping. Furthermore, the simplifications introduced by the vertical gravity–capillary equilibrium assumption allow efficient calculations of two-phase currents over distances required at the basin scale during geological sequestration of CO_2. In all these systems, and in a number of related areas, the incorporation of capillary effects provides new insight into the dynamics of two-phase gravity currents.

The authors would like to gratefully acknowledge the artistic expertise of Mark Hallworth. The research of M.J.G. is funded by the EPSRC, J.A.N. by the Leverhulme Trust and Lloyds Tercentenary Foundation, M.A.H. partly by a David Crighton Fellowship and the work of H.E.H. is partially supported by a Royal Society Wolfson Research Merit Award.

Appendix. Justification for vertical gravity–capillary equilibrium

Vertical gravity–capillary equilibrium is the key assumption of the two-phase gravity current model presented in this paper because it enables us to resolve the saturation

distribution within the current. In a long, thin gravity current, where flow is assumed to be predominately horizontal, we showed in § 3.1 that gravity–capillary equilibrium is implied by assuming that each phase is in hydrostatic equilibrium. However, the height of the current rises during propagation, so the saturation distribution, which depends on current height, must keep re-equilibrating in order for the assumption to remain valid. We find expressions for the time scale, t_m, over which the current height changes due to gravity-driven horizontal motion and the time scale, t_c, required for the saturation distribution to return to gravity–capillary equilibrium after a small change in current height. By showing that the ratio of time scales $r_t = t_c/t_m$ is small, we demonstrate that to a good approximation, gravity–capillary equilibrium is maintained as the current propagates. It should be noted that the assumption breaks down at the front of the current, where flow in the vertical direction is not negligible compared to the horizontal motion. However, this is the case in all gravity current models which consider long, thin currents and rely on the assumption of hydrostatic pressure. For example, Huppert (1982) showed experimentally for viscous gravity currents that it makes no difference to the overall motion of the current.

In order to find expressions for the time scales t_m and t_c, we vertically integrate the non-wetting phase local mass conservation equation (2.6) between z and h. This yields

$$\varphi \frac{\partial V(h,z)}{\partial t} + \frac{\partial}{\partial x}\int_z^h u_n \,\mathrm{d}z - [w_n]_z = 0, \tag{A 1}$$

where $V(h,z) = \int_z^h s(h,z')\,\mathrm{d}z'$ is the volume of fluid per unit length contained in a column of current that has height h, and we have used $s(z=h) = u_n(z=h) = w_n(z=h) = 0$.

The time scale, t_m, over which the current height changes due to the horizontal velocity of the current fluid during propagation is obtained from the balance between the first and second terms in (A 1). We make the assumption, as explained in § 3.1, that the current is in gravity–capillary equilibrium, and therefore we find that $\partial V/\partial t = s(h,z)\partial h/\partial t$ by using (3.4) and integrating directly. Darcy's law (2.7) provides an expression for horizontal velocity

$$u_n = -k\lambda_n(s)\frac{\partial p_n}{\partial x} = -\Delta\rho g k \lambda_n(s)\frac{\partial h}{\partial x}, \tag{A 2}$$

where the second equality comes from the expression for the hydrostatic non-wetting phase pressure, given by

$$p_n(h,z) = p_e + \rho_w g h - \rho_n g(h-z). \tag{A 3}$$

Note that this uses the condition $p_n = p_e + \rho_w g h$ at the current boundary $z = h$. We scale $t \sim t_m$, $z, h \sim H$ and $x \sim L$, where H and L are the characteristic length scales for the current height and horizontal extent, respectively, and write $\epsilon = H/L$. Hence, the first two terms of (A 1) yield the scaling

$$\varphi s \frac{H}{t_m} \sim \Delta\rho g k \lambda_n(s)\epsilon^2, \tag{A 4}$$

which we can rearrange to find an expression for the time scale, t_m, given by

$$t_m \sim \frac{\varphi H}{\Delta\rho g k}\frac{s}{\lambda_n(s)}\epsilon^{-2}. \tag{A 5}$$

Now we consider a current at height $h(x,t)$, which is in gravity–capillary equilibrium and therefore has saturation distribution $s(h,z)$, given by (3.4), and suppose that its height increases by δh. The time scale t_c indicates how quickly the recovery of vertical gravity–capillary equilibrium is achieved due to the vertical velocity of the non-wetting phase and is therefore given by the balance between the first and third terms in (A 1). Once gravity–capillary equilibrium is recovered, the saturation distribution is $s(h+\delta h,z)$, and therefore we find that

$$\delta V = V(h+\delta h,z) - V(h,z) = s(h,z)\delta h \tag{A 6}$$

to first order in δh. From (2.7) the vertical velocity, w_n, is given by

$$w_n = -k\lambda_n(s)\left(\frac{\partial p_n}{\partial z} - \rho_n g\right), \tag{A 7}$$

where the vertical gradient of the hydrostatic pressure $p_n(h+\delta h,z)$ after a change in height of δh can be written as

$$\frac{\partial p_n}{\partial z} = \frac{p_n(h+\delta h,h+\delta h) - p_n(h+\delta h,0)}{h} = \rho_n g\frac{(h+\delta h)}{h}. \tag{A 8}$$

Hence, (A 7) becomes

$$w_n = -\rho_n g k\lambda_n(s)\frac{\delta h}{h}. \tag{A 9}$$

We use (A 6) and (A 9) to scale $\partial V/\partial t \sim s(h,z)\delta h/t_c$ and $w_n \sim \rho_n g k\lambda_n(s)\delta h/h$ in (A 1) to find

$$\varphi s\frac{\delta h}{t_c} \sim \rho_n g k\lambda_n(s)\frac{\delta h}{H}, \tag{A 10}$$

which can be rearranged to give

$$t_c \sim \frac{\varphi H}{\rho_n g k}\frac{s}{\lambda_n(s)}. \tag{A 11}$$

Thus, we find, using (A 5) and (A 11), that the ratio of time scales

$$r_T \sim \frac{\Delta\rho}{\rho_n}\epsilon^2. \tag{A 12}$$

For a long, thin gravity current, $\epsilon \ll 1$, and so we have shown that vertical gravity–capillary equilibrium is recovered for a given change in current height on a time scale much smaller than the time scale of the overall motion of the current. We therefore conclude that the assumption of gravity–capillary equilibrium remains valid as the two-phase current propagates through the porous medium.

REFERENCES

Bear, J. & Ryzhik, V. 1998 On the displacement of NAPL lenses and plumes in a phreatic aquifer. *Trans. Porous Med.* **33**, 227–255.

Bear, J., Ryzhik, V., Braester, C. & Entov, V. 1996 On the movement of an LNAPL lens on the water table. *Trans. Porous Med.* **25**, 283–311.

Bennion, B. 2006 The impact of interfacial tension and pore-size distribution/capillary pressure character on CO_2 relative permeability at reservoir conditions in CO_2–brine systems. In *SPE/DOE Symposium on Improved Oil Recovery, Tulsa, Oklahoma, U.S.A., April 22–26*. (SPE 99325).

Bennion, B. & Bachu, S. 2005 Relative permeability characteristics for supercritical CO_2 displacing water in a variety of potential sequestration zones in the western Canada sedimentary basin. In *SPE Annual Technical Conference and Exhibition, Dallas, Texas, October 9–12*. SPE 95547.

Bickle, M., Chadwick, A., Huppert, H. E., Hallworth, M. & Lyle, S. 2007 Modelling carbon dioxide accumulation at Sleipner: implications for underground carbon storage. *Earth Planet. Sci. Lett.* **255**, 164–176.

Brooks, R. H. & Corey, A. T. 1964 Hydraulic properties of porous media. *Hydrology Papers* 3. Colorado State University.

Bryant, S. L., Lakshminarasimhan, S. & Pope, G. A. 2008 Buoyancy-dominated multiphase flow and its effect on geological sequestration of CO_2. *Soc. Petrol. Engng J.* **13** (4), 447–454.

Corey, A. T. 1954 The interrelation between gas and oil relative permeabilities. *Prod. Monthly* **19 (1)**, 38–41.

Ennis-King, J. & Paterson, L. 2005 Role of convective mixing in the long-term storage of carbon dioxide in deep saline formations. *Soc. Petrol. Engng J.* **10** (3), 349–356.

Farcas, A. & Woods, A. W. 2009 The effect of drainage on the capillary retention of CO_2 in a layered permeable rock. *J. Fluid Mech.* **618**, 349–359.

Fetter, C. W. 2001 *Applied Hydrogeology*. Prentice-Hall.

Gasda, S. E., Bachu, S. & Celia, M. A. 2004 Spatial characterization of the location of potentially leaky wells penetrating a deep saline aquifer in a mature sedimentary basin. *Environ. Geol.* **46**, 707–720.

Gasda, S. E., Nordbotten, J. M. & Celia, M. A. 2009 Vertical equilibrium with sub-scale analytical methods for geological CO_2 sequestration. *Comput. Geosci.* **13**, 469–481.

van Genuchten, M. Th. 1980 A closed-form equation for predicting the hydraulic conductivity of unsaturated soils. *Soil Sci. Soc. Am. J.* **44**, 892–898.

Golding, M. J. & Huppert, H. E. 2010 The effect of confining impermeable boundaries on gravity currents in a porous medium. *J. Fluid Mech.* **649**, 1–17.

Green, C. P. & Ennis-King, J. 2010 Effect of vertical heterogeneity on long-term migration of CO_2 in saline formations. *Trans. Porous Med.* **82**, 31–47.

Hesse, M. A., Orr, Jr, F. M. & Tchelepi, H. A. 2008 Gravity currents with residual trapping. *J. Fluid Mech.* **611**, 35–60.

Hesse, M. A., Tchelepi, H. A., Cantwell, B. J. & Orr, Jr, F. M. 2007 Gravity currents in horizontal porous layers: transition from early to late self-similarity. *J. Fluid Mech.* **577**, 363–383.

Hesse, M. A. & Woods, A. W. 2010 Buoyant dispersal of CO_2 during geological storage. *Geophys. Res. Lett.* **37**, L01403.

Huppert, H. E. 1982 The propagation of two-dimensional and axisymmetric viscous gravity currents over a rigid horizontal surface. *J. Fluid Mech.* **121**, 43–58.

Huppert, H. E. & Woods, A. W. 1995 Gravity-driven flows in porous layers. *J. Fluid Mech.* **292**, 55–69.

Ide, S. T., Jessen, K. & Orr, Jr, F. M. 2007 Storage of CO_2 in saline aquifers: effects of gravity, viscous, and capillary forces on amount and timing of trapping. *Intl J. Greenh. Gas Control* **1**, 481–491.

Johnson, J. W., Nitao, J. J & Knauss, K. G. 2004 Reactive transport modelling of CO_2 storage in saline aquifers to elucidate fundamental processes, trapping mechanisms and sequestration partitioning. In *Geological Storage of Carbon Dioxide* (ed. S. J. Baines & R. H. Worden). The Geological Society of London.

Juanes, R., MacMinn, C. W. & Szulczewski, M. L. 2010 The footprint of the CO_2 plume during carbon dioxide storage in saline aquifers: storage efficiency for capillary trapping at the basin scale. *Trans. Porous Med.* **82**, 19–30.

Juanes, R., Spiteri, E. J., Orr, Jr, F. M. & Blunt, M. J. 2006 Impact of relative permeability hysteresis on geological CO_2 storage. *Water Resour. Res.* **42**, W12418.

Kochina, I. N., Mikhailov, N. N. & Filinov, M. V. 1983 Groundwater mound damping. *Intl J. Engng Sci.* **21** (4), 413–421.

Kumar, A., Ozah, R., Noh, M., Pope, G. A., Bryant, S., Sepehrnoori, K. & Lake, L. W. 2005 Reservoir simulation of CO_2 storage in deep saline aquifers. *Soc. Petrol. Engng J.* **10** (3), 336–348.

Lake, L. W. 1996 *Enhanced Oil Recovery*. Prentice-Hall.

Land, C. S. 1968 Calculation of imbibition relative permeability for two- and three-phase flow from rock properties. *Soc. Petrol. Engng J.* **8(2)**, 149–156.

Lenormand, R., Zarcone, C. & Sarr, A. 1983 Mechanisms of the displacement of one fluid by another in a network of capillary ducts. *J. Fluid Mech.* **135**, 337–353.

Leverett, M. C. 1939 Flow of oil–water mixtures through unconsolidated sands. *Trans. AIME* **132**, 149–171.

Leverett, M. C. 1941 Capillary behavior in porous solids. *Trans. AIME* **142**, 152–169.

Li, K. & Horne, R. N. 2006 Comparison of methods to calculate relative permeability from capillary pressure in consolidated water-wet porous media. *Water Resour. Res.* **42**, W06405.

MacMinn, C. W. & Juanes, R. 2009 Post-injection spreading and trapping of CO_2 in saline aquifers: impact of the plume shape at the end of injection. *Comput. Geosci.* **13**, 483–491.

Metz, B., Davidson, O., de Coninck, H., Loos, M. & Meyer, L., (Ed.) 2005 *IPCC Special Report on Carbon Dioxide Capture and Storage*. Cambridge University Press, prepared by Working Group III of the Intergovernmental Panel on Climate Change.

Mo, S., Zweigel, P., Lindeberg, E. & Akervoll, I. 2005 Effect of geologic parameters on CO_2 storage in deep saline aquifers. In *SPE Eurospec/EAGE Annu. Conf., Madrid, Spain, June 13–16*. SPE 93952.

Neufeld, J. A. & Huppert, H. E. 2009 Modelling carbon dioxide sequestration in layered strata. *J. Fluid Mech.* **625**, 353–370.

Neufeld, J. A., Vella, D. & Huppert, H. E. 2009 The effect of a fissure on storage in a porous medium. *J. Fluid Mech.* **639**, 239–259.

Nordbotten, J. M. & Celia, M. A. 2006 Similarity solutions for fluid injection into confined aquifers. *J. Fluid Mech.* **561**, 307–327.

Nordbotten, J. M., Celia, M. A., Bachu, S. & Dahle, H. K 2005 Semianalytical solution for CO_2 leakage through an abandoned well. *Environ. Sci. Technol.* **39** (2), 602–611.

Parker, J. C. & Lenhard, R. J. 1989 Vertical integration of three-phase flow equations for analysis of light hydrocarbon plume movement. *Trans. Porous Med.* **5**, 187–206.

Pentland, C. H., Al-Mansoori, S., Iglauer, S., Bijeljic, B. & Blunt, M. J. 2008 Measurement of non-wetting phase trapping in sand packs. In *SPE Annual Technical Conf. and Exhibition, Denver, CO*. SPE 115697.

Pinder, G. F. & Gray, W. G. 2008 *Essentials of Multiphase Flow and Transport in Porous Media*. Wiley.

Riaz, A. & Tchelepi, H. A. 2006 Numerical simulation of immiscible two-phase flow in porous media. *Phys. Fluids* **18**, 014104.

Saadatpoor, E., Bryant, S. L. & Sepehrnoori, K. 2010 New trapping mechanisms in carbon sequestration. *Trans. Porous Med.* **82**, 3–17.

Vella, D. & Huppert, H. E. 2006 Gravity currents in a porous medium at an inclined plane. *J. Fluid Mech.* **555**, 353–362.

Woods, A. W. & Farcas, A. 2009 Capillary entry pressure and the leakage of gravity currents through a sloping layered permeable rock. *J. Fluid Mech.* **618**, 361–379.

Yortsos, Y. C. 1995 A theoretical analysis of vertical flow equilibrium. *Trans. Porous Med.* **18** (2), 107–129.